Kinetics of the $C_3H_7O_2$ + NO Reaction: Temperature Dependence of the Overall Rate Constant and the *i*-$C_3H_7ONO_2$ Branching Channel

Jessica M. Chow, Angela M. Miller, and Matthew J. Elrod*

Department of Chemistry, Oberlin College, Oberlin, Ohio 44074

Received: May 17, 2002; In Final Form: November 22, 2002

The temperature dependence of the overall rate constant for the $C_3H_7O_2$ + NO reaction and the rate constant for the minor branching channel resulting in the production of *i*-$C_3H_7ONO_2$ have been measured using the turbulent flow technique with high-pressure chemical ionization mass spectrometry for the detection of reactants and products. The temperature dependence of the overall rate constant for the $C_3H_7O_2$ + NO reaction was investigated between 298 and 213 K at 100 Torr pressure, and the data were fit by the following Arrhenius expression (with 2 standard deviation error limits indicated): $4.3^{+1.0}_{-0.9} \times 10^{-12}$ exp[(268 ± 56)/*T*] cm^3 molecule^{-1} s^{-1}. This expression agrees well with previous isomer-specific measurements of the *n*-$C_3H_7ONO_2$ and *i*-$C_3H_7O_2$ + NO rate constants made at lower pressures. The temperature dependence of the rate constant for the minor reaction channel *i*-$C_3H_7O_2$ + NO → *i*-$C_3H_7ONO_2$ was investigated between 298 and 213 K at 100 Torr pressure. The following Arrhenius expression was determined for the minor channel: $4.9^{+5.3}_{-2.9} \times 10^{-16}$ exp[(1380 ± 230)/*T*] cm^3 molecule^{-1} s^{-1}. The Arrhenius expressions for the overall rate and the *i*-$C_3H_7ONO_2$ producing channel indicate a branching ratio of about 0.006 at 298 K and 0.020 at 213 K at 100 Torr pressure, which is in good agreement with the predictions of a recently revised empirical model for alkyl nitrate branching ratios.

Introduction

Alkyl peroxy radicals (RO_2) are important intermediate species formed in the oxidation of alkanes in the atmosphere[1]

$$RH + OH \rightarrow R + H_2O \quad (1)$$

$$R + O_2 + M \rightarrow RO_2 + M \quad (2)$$

Ozone levels in the atmosphere are directly affected by RO_2 reactions, and the identity of the dominant RO_2 reactions are dependent on the levels of the nitrogen oxides (NO_x). Under high NO_x conditions (generally, lower tropospheric urban conditions), RO_2 reactions lead to the production of ozone, the most deleterious constituent of photochemical smog

$$RO_2 + NO \rightarrow RO + NO_2 \quad (3a)$$

$$NO_2 + h\nu\ (\lambda < 420\ \text{nm}) \rightarrow NO + O \quad (4)$$

$$O + O_2 + M \rightarrow O_3 + M \quad (5)$$

RO_2 can also be temporarily removed from ozone production cycles by the formation of reservoir species such as the alkyl nitrates

$$RO_2 + NO + M \rightarrow RONO_2 + M \quad (3b)$$

Because reaction 3b removes the radical chain carrier RO_2 from the ozone production cycle, it has a direct effect on the ozone-producing efficiency of the RH/NO_x system.

Atkinson and co-workers have developed an empirical relationship for the yield of the secondary organic nitrates from reaction 3 from the results of environmental chamber photolysis studies of C_3-C_8 *n*-alkanes.[2] The branching ratio [$k_{3b}/(k_{3a} + k_{3b})$] is found to rise from 0.039 for the propyl case to 0.23 for the *n*-octyl case at 298 K and 740 torr, thus indicating the importance of the association channel 3b, particularly for the larger alkyl peroxy radicals. The model can also be used to predict the branching ratios for primary and tertiary nitrate formation through the use of a scaling factor based on the available results for experimental primary and tertiary systems.[3] However, the experimental data is less extensive for these species, and the predictions are expected to be less accurate.

In previous work, we extended the experimental measurements to the C_1 and C_2 alkanes by measuring the overall rate constant (k_3) for the CH_3O_2 [4] and $C_2H_5O_2$ [5] + NO reactions, as well as values for the nitrate branching ratios. Our experimental results for the $C_2H_5ONO_2$ branching ratio were in only fair agreement with the predictions from the Atkinson model. Therefore, the goal of this work is to extend our experimental measurements to the C_3 system to assess whether the $C_2H_5ONO_2$ inconsistencies are due to a specific inaccuracy in the Atkinson model[3] for this primary nitrate, or whether there might exist a more general systematic discrepancy between the experimental methods employed (which would be revealed by a differing result for the $C_3H_7ONO_2$ branching ratio).

Reaction 1 leads to two possible alkyl radical isomers for the case of the C_3H_8 + OH reaction. It has been shown that the distribution of alkyl radicals isomers at 295 K is about 75% *i*-C_3H_7 and 25% *n*-C_3H_7.[6] There have been several previous kinetics investigations of the overall rate of reaction of $C_3H_7O_2$ + NO.[7−11] It has been well established that the reaction

$$C_3H_7O_2 + NO \rightarrow C_3H_7O + NO_2 \quad (6a)$$

is the predominant channel. In particular, the more recent work

* To whom correspondence should be addressed. Phone: (440) 775-6583. Fax: (801) 697-4917. E-mail: matthew.elrod@oberlin.edu.

10.1021/jp026134b CCC: $25.00
Published on Web 04/03/2003

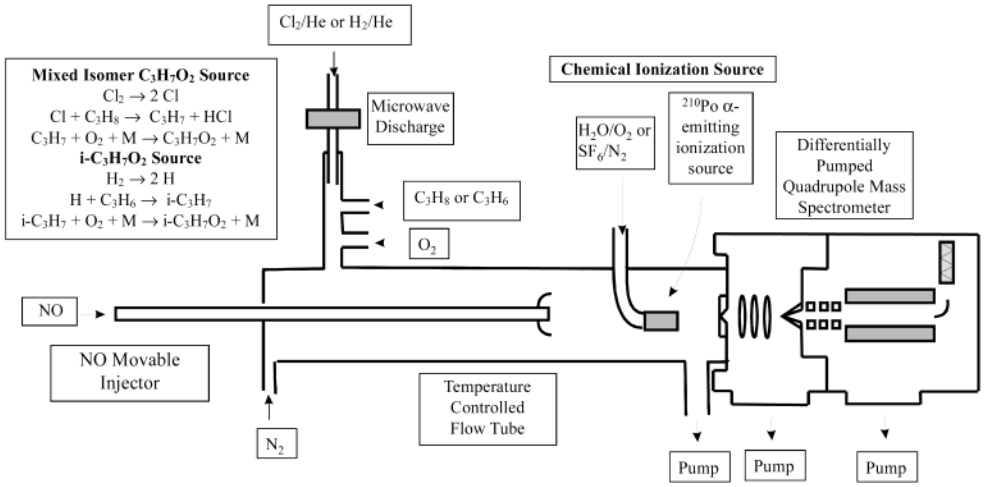

Figure 1. Experimental apparatus.

of Howard and co-workers have established that the overall rate constant is identical for the two possible propyl peroxy isomers, *n*-$C_3H_7O_2$ and *i*-$C_3H_7O_2$, with a value of 9.0×10^{-12} cm^3 molecule^{-1} s^{-1} at 298 K and pressures near 1 Torr.[8,9]

The minor nitrate-forming channel for the $C_3H_7O_2$ + NO reaction is

$$C_3H_7O_2 + NO + M \rightarrow C_3H_7ONO_2 + M \qquad (6b)$$

In 1982, using an environmental smog chamber, Atkinson and co-workers first measured the secondary propyl nitrate (*i*-$C_3H_7ONO_2$) branching ratio [$k_{6b}/(k_{6a} + k_{6b})$] to be 0.036 at 299 K and 735 torr.[12] Based on more recent estimates for the propyl radical distribution resulting from the reaction of propane and OH, Arey et al. recently adjusted the secondary propyl nitrate branching ratio to a value of 0.039.[2] More importantly, new measurements of the C_6-C_8 systems were performed, and new parameters for the temperature and pressure dependent empirical model were also established.[2] The new model predicts the secondary propyl nitrate branching ratio at 299 K and 735 torr to be 0.041, in good agreement with the experimental results. Although the overall rate constants for the different $C_3H_7O_2$ isomers in reaction 6a were found by Howard and co-workers to be identical, the work of Atkinson and co-workers has shown that there is a clear isomer dependence in the nitrate branching ratios for the entire C_3-C_8 series. Therefore, it is important to use methods that are selective for the specific isomers in the nitrate branching ratio studies.

Bertman et al. have proposed that the alkyl nitrate branching ratios can be used in regional atmospheric models that determine the air mass age from observations of the relative concentration of alkyl nitrate to the parent alkane.[13] Although their method was found to be self-consistent for the secondary C_4 and C_5 nitrates, Bertman et al. found that their model systematically underpredicted measured ethyl and propyl nitrate levels by a substantial amount. There are two potential explanations for this result: (1) the experimental alkyl nitrate branching ratios are too low or (2) ethyl and propyl nitrates are also formed after the decomposition of larger alkoxy radicals, leading to higher amounts of these alkyl nitrates than predicted from the atmospheric levels of ethane and propane. In previous work, using our experimental results for the $C_2H_5ONO_2$ branching ratio and the Bertman et al. model, we supported the contention that most $C_2H_5ONO_2$ present in the atmosphere is not a result of ethane oxidation chemistry.[5]

In this article, we describe our investigation of the kinetics of the $C_3H_7O_2$ + NO reaction conducted at pressures near 100 Torr and at a range of temperatures extending to those found in the lower stratosphere using a turbulent flow (TF) tube coupled to a high pressure chemical ionization mass spectrometer (CIMS). It has been previously shown that the TF technique can be used to accurately determine the rate constants of reactions at pressures ranging from 50 to 760 Torr and at temperatures as low as 180 K.[14,15] As in our previous kinetics studies of CH_3O_2 + NO[4] and $C_2H_5O_2$ + NO[5] using the coupled TF−CIMS approach, we are able to directly access atmospheric pressure and temperature conditions and sensitively monitor many of the relevant reactants and products for the $C_3H_7O_2$ + NO reaction. In the $C_2H_5O_2$ + NO work, the TF−CIMS kinetics technique was used in the determination of the temperature-dependent overall rate constant and the first measurement of the $C_2H_5ONO_2$ producing channel for this reaction,[5] thus improving on a previous estimate for the upper limit of this process at room temperature and atmospheric pressure.[12] In this article, we describe a similar temperature-dependent kinetics investigation of the overall rate constant and the measurement of the *i*-$C_3H_7ONO_2$ producing channel (the dominant propyl nitrate-forming reaction) rate constant for the *i*-$C_3H_7O_2$ + NO reaction.

Experimental Section

Turbulent Fast Flow Kinetics. A schematic of the experimental apparatus is presented in Figure 1 and is similar to that used in our previous study of $C_2H_5O_2$ + NO_x.[5] The flow tube was constructed with 2.2 cm i.d. Pyrex tubing and was 100 cm in total length. A large flow of nitrogen carrier gas (approximately 30 STP L min^{-1}) was injected at the rear of the flow tube. The gases necessary to generate $C_3H_7O_2$ were introduced though a 10 cm long 12.5 mm diameter sidearm located at the rear of the tube. NO was added via an encased movable injector. The encasement (made from corrugated Teflon tubing) was used so that the injector could be moved to various injector positions without breaking any vacuum seals, as well as to prevent ambient gases from condensing on cold portions of the injector. A fan-shaped Teflon device was placed at the end of the injector in order to enhance turbulent mixing. The polonium-210 alpha-emitting ionization source was placed between the temperature regulated flow tube and the inlet to the CIMS. Most of the flow tube gases were removed at the CIMS inlet by a 31 L s^{-1} roughing pump. All gas flows were monitored with calibrated mass flow meters. The flow tube pressure was measured upstream of the ionization source using a 0−1000 Torr capacitance manometer. The temperature was

determined at both the entrance and exit points of the temperature regulated region of the flow tube using Cu-constantan thermocouples.

Overall Rate Constant Determination. $C_3H_7O_2$ (all molecules mentioned are mixed isomers, unless otherwise indicated) was generated using the following reactions:

$$C_3H_8 + Cl \rightarrow C_3H_7 + HCl \quad (7)$$

$$C_3H_7 + O_2 + M \rightarrow C_3H_7O_2 + M \quad (8)$$

($k_7 = 1.37 \times 10^{-10}$ cm^3 molecule^{-1} s^{-1} and $k_8 = 1.1 \times 10^{-11}$ cm^3 molecule^{-1} s^{-1} at 100 Torr; all rate constant values quoted are for 298 K unless otherwise indicated).[16,17] Chlorine atoms were produced by passing a dilute Cl_2/He mixture through a microwave discharge produced by a Beenakker cavity operating at 50 W. The dilute Cl_2/He mixture was obtained by combining a 2.0 STP L min^{-1} flow of helium (99.999%), which had passed through a silica gel trap immersed in liquid nitrogen, with a 0.5−5.0 STP mL min^{-1} flow of a 1% Cl_2 (99.9%)/He mixture. To generate C_3H_7, the chlorine atoms were then injected into a sidearm and mixed with an excess of C_3H_8 (CP grade, $\sim 2 \times 10^{14}$ molecule cm^{-3}) in order to ensure that no chlorine atoms were introduced into the main flow. $C_3H_7O_2$ was then produced by the addition of a large excess of O_2 (99.995%; $>2.0 \times 10^{16}$ molecule cm^{-3}) just downstream of the production of C_3H_7. Absolute $C_3H_7O_2$ concentrations (needed to ensure pseudo-first-order kinetics conditions and for branching ratio modeling) were determined by the titration of $C_3H_7O_2$ with NO (see $C_3H_7ONO_2$ Branching Channel Reactant Preparation section). To ensure pseudo-first-order kinetics conditions, the main flow tube $C_3H_7O_2$ concentrations ranged from 5.0 to 10×10^{10} molecules cm^{-3}. The C_3H_8 + Cl reaction also leads to a similar *i*-C_3H_7-dominated isomer distribution,[18] as is the case for the C_3H_8 + OH reaction. Thus, our overall rate constant measurements represent a weighted average value for the two isomers.

For the overall rate determination for the $C_3H_7O_2$ + NO reaction, NO was added to the flow reactor as a 1% mixture in N_2 through the movable injector. To ensure the absence of NO_2 impurities, NO was passed through a silica gel trap held at −78 C. Negligible NO_2 concentrations were observed via CIMS methods.

For the low-temperature studies, liquid-nitrogen-cooled silicone oil was used as the coolant for the jacketed flow tube. Nitrogen carrier gas was precooled by passing it through a copper coil immersed in a liquid N_2 reservoir followed by resistive heating. The temperature was controlled in the reaction region to within 1 K. The pressure was maintained at approximately 100 Torr in order to achieve optimum instrument performance. Pressures below 100 Torr were found to lower the ionization efficiency, and pressures above 100 Torr were found to lower the radical production efficiency.

***i*-$C_3H_7ONO_2$ Branching Channel Reactant Preparation.** *i*-$C_3H_7O_2$ was selectively generated using the following reactions:

$$H + C_3H_6 \rightarrow i\text{-}C_3H_7 \quad (9)$$

$$i\text{-}C_3H_7 + O_2 + M \rightarrow i\text{-}C_3H_7O_2 + M \quad (10)$$

($k_9 = 2.0 \times 10^{-12}$ cm^3 molecule^{-1} s^{-1} and $k_{10} = 1.1 \times 10^{-11}$ cm^3 molecule^{-1} s^{-1} at 100 Torr).[17,19] H atoms were produced by passing a dilute H_2/He mixture through a microwave discharge produced by a Beenakker cavity operating at 50 W. The dilute H_2/He mixture was obtained by combining 2.0 STP L min^{-1} flow of helium (99.999%), which had passed through a silica gel trap immersed in liquid nitrogen, with a 0.4 STP mL min^{-1} flow of a 1% H_2 (99.9%)/He mixture. To generate *i*-C_3H_7, the hydrogen atoms were then injected into a sidearm and mixed with an excess of C_3H_6 (CP grade, $\sim 2 \times 10^{14}$ molecule cm^{-3}) in order to ensure that no hydrogen atoms were introduced into the main flow. *i*-$C_3H_7O_2$ was then produced by the addition of a large excess of O_2 to the main flow (99.995%; $>5.0 \times 10^{17}$ molecule cm^{-3}) at the intersection of the sidearm and the main flow tube. Absolute *i*-$C_3H_7O_2$ concentrations were determined by the titration of NO to produce *i*-C_3H_7O and NO_2

$$i\text{-}C_3H_7O_2 + NO \rightarrow i\text{-}C_3H_7O + NO_2 \quad (11a)$$

($k_{11a} = 9.0 \times 10^{-12}$ cm^3 molecule^{-1} s^{-1})[9] and subsequent calibration of the NO_2 mass spectrometer signal. 0.5 % NO_2/N_2 mixtures were used as standard samples for mass spectrometric calibration. Computer modeling of the reactions occurring during the titration indicated that not all of the *i*-$C_3H_7O_2$ initially present was converted to the stable species, NO_2. This is mainly due to reactions of *i*-$C_3H_7O_2$ with other species in the chemical system (which will be addressed in the discussion section). Therefore, the *i*-$C_3H_7O_2$ concentrations were calculated from the NO_2 concentrations by explicitly determining the conversion factor (usually ~0.9) from computer modeling using the specific experimental conditions. As mentioned in the previous section, NO was purified *in situ* by passing it through a silica gel trap held at −78 C. For this study, *i*-$C_3H_7O_2$ concentrations ranged from 3.0 to 7.0×10^{11} molecule cm^{-3}.

***i*-$C_3H_7ONO_2$ Branching Channel Measurements.** In these studies, the production of *i*-$C_3H_7ONO_2$ from reaction 11b

$$i\text{-}C_3H_7O_2 + NO \rightarrow i\text{-}C_3H_7ONO_2 \quad (11b)$$

was directly monitored over a reaction time of ~30 ms. Computer modeling was used to extract the rate constant k_{11b} from the observed production of *i*-$C_3H_7ONO_2$ and initial concentrations of all relevant chemical species. As will be discussed in the Results and Discussion section, both the time profile of the *i*-$C_3H_7ONO_2$ production and the absolute amount of *i*-$C_3H_7ONO_2$ produced over the longest reaction time were used as constraints on the determination of k_{11b}; therefore, it was critical that the absolute *i*-$C_3H_7ONO_2$ concentrations were determined accurately. Standard samples of *i*-$C_3H_7ONO_2$ (Aldrich, 96%) for mass spectrometric calibration were commercially obtained and prepared by drawing an appropriate amount of *i*-$C_3H_7ONO_2$ vapor from the liquid sample, followed by mixing with N_2 to make 0.5% *i*-$C_3H_7ONO_2$ mixtures appropriate for mass spectrometric calibration.

To aid in the detection of the *i*-$C_3H_7ONO_2$ product, higher *i*-$C_3H_7O_2$ were used for the branching ratio measurements than in the determination of the bimolecular rate constant (because *i*-$C_3H_7O_2$ is the limiting reagent). The major complication in the branching ratio determination is from the reaction of the *i*-C_3H_7O radical (formed in reaction 11a) with NO_2

$$i\text{-}C_3H_7O + NO_2 + M \rightarrow i\text{-}C_3H_7ONO_2 + M \quad (12)$$

($k_{12} = 3.3 \times 10^{-11}$ cm^3 molecule^{-1} s^{-1} at 100 Torr).[20] Reaction 12 is therefore a potential source of *i*-$C_3H_7ONO_2$, and experimental conditions must be designed to minimize this relatively fast reaction. By keeping O_2 concentrations very high, computer modeling indicates that the reaction

$$i\text{-}C_3H_7O + O_2 \rightarrow CH_3C(O)CH_3 + HO_2 \quad (13)$$

($k_{13} = 6.5 \times 10^{-15}$ cm^3 molecule^{-1} s^{-1})[20,21] will consume most of the *i*-C_3H_7O produced by reaction 11a and minimize production of *i*-$C_3H_7ONO_2$ by reaction 12. This reaction is slightly less efficient (5.2×10^{-15} cm^3 molecule^{-1} s^{-1} at 213 K) at the lowest temperatures used in this study.

To drive the production of *i*-$C_3H_7ONO_2$ from reaction 12 down to very low levels, O_2 was added to the flow tube at concentrations of $\sim 5.0 \times 10^{17}$ molecule cm^{-3}. Additional experiments were performed with O_2 concentrations of 1.0×10^{18} molecule cm^{-3} in order to investigate potential interferences from this reaction.

Chemical Ionization Mass Spectrometric Detection. Positive ion chemical ionization schemes (with $H^+(H_2O)_n$ as the reagent ion) were used to detect *i*- and *n*-$C_3H_7O_2$ and *i*-$C_3H_7ONO_2$, and negative ion chemical ionization schemes (with SF_6^- as the reagent ion) were used to detect NO_2 with the quadrupole mass spectrometer. $H^+(H_2O)_n$ (with the $n = 4$ species usually accounting for more than 80% of the total ion signal) was produced in the ion source by passing a large O_2 flow (8 STP L min^{-1}) through the polonium-210 alpha-emitting ionization source (with H_2O impurities being sufficiently abundant to produce adequate quantities of reagent ions). SF_6^- was produced in the ion source by passing a large N_2 flow (9 STP L min^{-1}) and 1.0 STP mL min^{-1} of 10% SF_6/N_2 through the ionization source. The commercial ionization source consisted of a hollow cylindrical (69 by 12.7 mm) aluminum body with 10 mCurie (3.7×10^8 disintegrations s^{-1}) of polonium-210 coated on the interior walls.

Ions were detected with a quadrupole mass spectrometer housed in a two-stage differentially pumped vacuum chamber. Flow tube gases (neutrals and ions) were drawn into the front chamber through a charged 0.1 mm aperture. The ions were focused by three lenses constructed from 3.8 cm i.d. and 48 cm o.d. aluminum gaskets. The front chamber was pumped by a 6 in. 2400 L s^{-1} diffusion pump. The gases entered the rear chamber through a skimmer cone with a charged 1.0 mm orifice which was placed approximately 5 cm from the front aperture. The rear chamber was pumped by a 250 L s^{-1} turbomolecular pump. Once the ions passed through the skimmer cone, they were mass filtered and detected with a quadrupole mass spectrometer.

Chemical Ionization Schemes. Because the chemical ionization reactions are not expected to be sensitive to the isomeric structure of the neutral species under study and the mass spectrometric method is incapable of distinguishing between isomers, the ion−molecule reactions are discussed below in an isomer-neutral fashion. To perform pseudo-first-order kinetics studies of the overall rate of reaction 6, a chemical ionization scheme for $C_3H_7O_2$ is required. In our previous study of the CH_3O_2 + NO reaction,[4] we developed the following chemical ionization detection scheme for CH_3O_2 based on the computational thermodynamic prediction[22] that CH_3O_2 has a higher proton affinity than H_2O

$$CH_3O_2 + H^+(H_2O)_4 \rightarrow CH_3OOH^+(H_2O)_3 + H_2O \quad (14)$$

Because the proton affinity of $C_3H_7O_2$ is expected to be very similar to CH_3O_2, we successfully attempted to detect $C_3H_7O_2$ with the analogous reaction

$$C_3H_7O_2 + H^+(H_2O)_4 \rightarrow C_3H_7OOH^+(H_2O)_3 + H_2O \quad (15)$$

To perform branching ratio measurements for reaction 11b, chemical ionization schemes are needed for NO_2 (to determine the *i*-$C_3H_7O_2$ concentration) and for the product *i*-$C_3H_7ONO_2$.

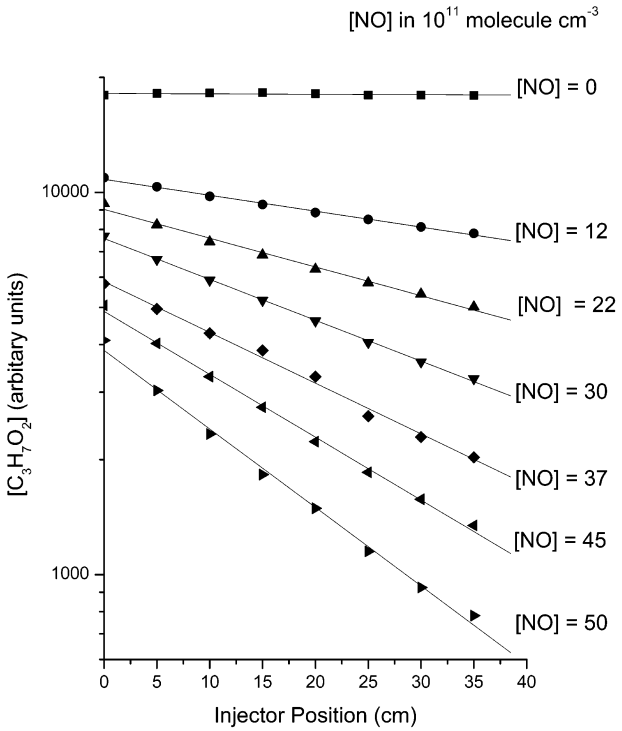

Figure 2. Pseudo-first-order $C_3H_7O_2$ decay curves for the $C_3H_7O_2$ + NO reaction at 100 Torr, 298 K, and 1170 cm s^{-1} velocity.

NO_2 was detected using a previously reported SF_6^- chemical ionization scheme

$$NO_2 + SF_6^- \rightarrow NO_2^- + SF_6 \quad (16)$$

($k_{16} = 1.4 \times 10^{-10}$ cm^3 molecule^{-1} s^{-1}).[23] We found that *i*-$C_3H_7ONO_2$ reacts very quickly with $H^+(H_2O)_4$

$$C_3H_7ONO_2 + H^+(H_2O)_4 \rightarrow C_3H_7ONO_2 \cdot H^+(H_2O)_3 + H_2O \quad (17)$$

such that high sensitivity could be achieved for the detection of this important product. The detection sensitivity of *i*-$C_3H_7ONO_2$ was estimated to be about 100 ppt at 100 Torr.

Results and Discussion

Overall Rate Constant Determination. Bimolecular rate constants were obtained via the usual pseudo-first-order approximation method, using NO as the excess reagent. Typical $C_3H_7O_2$ decay curves as a function of injector distance are shown in Figure 2 for the NO kinetics measurements. The first-order rate constants obtained from fitting the $C_3H_7O_2$ decay curves were plotted against [NO] in order to determine the bimolecular rate constant, as shown in Figure 3. This approach for determining bimolecular rate constants assumes that deviations from the plug flow approximation (molecular velocities are equal to the bulk flow velocity) are negligible. Under the conditions present in our turbulent flow tube (Reynold's number >2000), Seeley et al. estimated that these deviations result in apparent rate constants which are at most 8% below the actual values.[14] A portion of the plug flow deviation can be traced to the diffusivity contribution to the flow continuity equation. Because both eddy diffusion and molecular diffusion contribute roughly equally to the diffusivity term, it is possible that turbulent flow kinetics studies using molecules with smaller diffusion coefficients (such as $C_3H_7O_2$ in this case, as compared to the H atom studies carried out by Seeley et al.) might lead

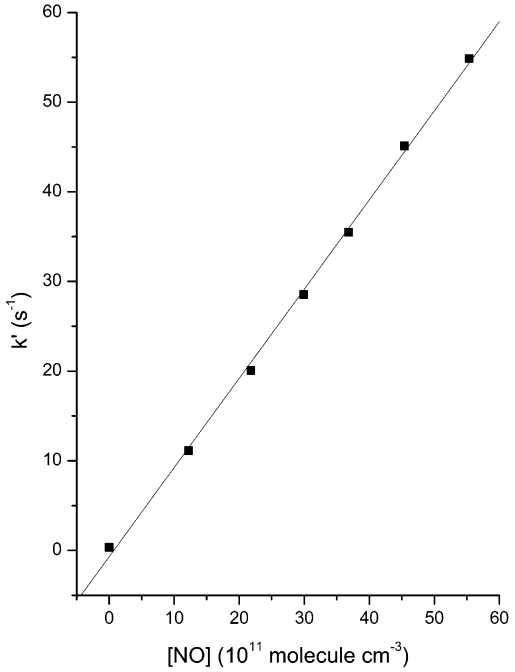

Figure 3. Determination of overall bimolecular rate constant for the $C_3H_7O_2$ + NO reaction from data in Figure 2.

TABLE 1: Overall Rate Constant Data for the $C_3H_7O_2$ + NO Reaction at 100 Torr Pressure

T (K)	velocity (cm s^{-1})	Reynolds number	k_6 [a] (10^{-12} cm^3 molecule^{-1} s^{-1})
298	1160	2190	11.2 ± 1.9
298	1150	2220	10.5 ± 0.7
298	1170	2200	9.8 ± 1.6
288	1250	2500	11.4 ± 0.9
288	1280	2580	11.9 ± 0.9
288	1300	2560	11.3 ± 1.6
273	1060	2290	11.9 ± 0.8
273	1060	2290	10.4 ± 0.7
263	970	2200	11.7 ± 1.4
263	991	2330	12.2 ± 0.9
253	974	2500	11.9 ± 0.7
253	957	2470	12.9 ± 1.0
243	906	2480	12.1 ± 1.4
243	923	2470	11.9 ± 1.8
243	916	2450	13.3 ± 1.9
243	916	2450	13.3 ± 0.2
233	960	2580	15.1 ± 1.2
233	955	2730	14.2 ± 0.7
233	955	2730	13.9 ± 0.5
223	961	2970	13.8 ± 1.3
223	970	2930	15.4 ± 1.1
213	966	3260	14.7 ± 3.4
213	966	3260	15.3 ± 1.3

[a] Stated error is 2σ.

to larger plug flow deviations. However, because the flow is modified by the use of a device (the "turbulizer" described in the Experimental Section) to enhance turbulent mixing, the plug flow approximation might be more exact for our conditions than a numerical simulation of the basic turbulent flow dynamics might suggest. Nontheless, it continues to be important to confirm the plug flow validity of the turbulent flow method via inspection of the pseudo-first-order decays and by comparison to other experimental methods. The other likely systematic errors in the determination of rate constants are likely to occur in the measurements of gas flows, temperature, detector signal, and pressure. Considering such sources of error, we

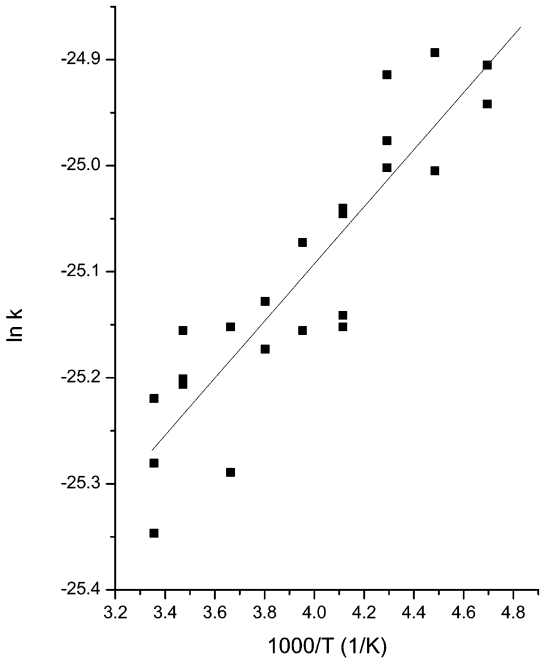

Figure 4. Arrhenius plot of the temperature dependence of the overall rate constant for the $C_3H_7O_2$ + NO reaction.

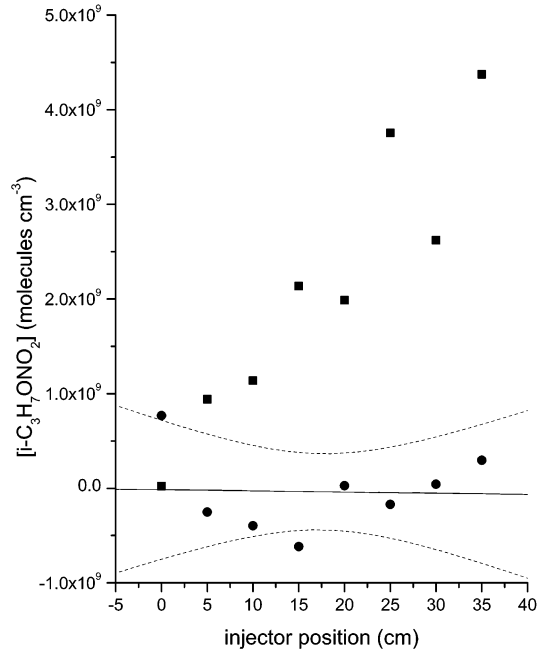

Figure 5. Observed production of i-$C_3H_7ONO_2$ from reaction 6b (squares) above the i-$C_3H_7ONO_2$ background level (circles) as a function of injector distance. A least squares fit to the background level was performed, and the dotted lines represent the 2σ level. This data set was obtained under the following conditions: $P = 100$ Torr, $T = 223$ K, velocity = 1180 cm s^{-1}, Reynold's number = 3660, $[i\text{-}C_3H_7O_2]_0 = 3.40 \times 10^{11}$ molecule cm^{-3}, $[NO]_0 = 4.56 \times 10^{12}$ molecule cm^{-3}.

estimate that rate constants can be determined with an accuracy of ±30% (2σ).

We performed several determinations of the rate constant at 100 Torr and 298 K for the mixed isomer $C_3H_7O_2$ + NO reaction (see Table 1 for a complete list of experimental conditions and measured rate constants) and arrived at the mean value of $k = (10.5 \pm 1.4) \times 10^{-12}$ cm^3 molecule^{-1} s^{-1}; the uncertainty represents the two standard deviation statistical errors in the data and is not an estimate of systematic errors. Our room-temperature constant is in excellent agreement with previous

TABLE 2: Kinetics Parameters for Branching Ratio Determination[p]

reaction	A (cm^3 s^{-1} $molecule^{-1}$)	E_a/R (K)	k_o^{300} (cm^6 s^{-1} $molecule^{-2}$)	m	k_∞^{300} (cm^3 s^{-1} $molecule^{-1}$)	n
i-$C_3H_7O_2$ + NO → i-C_3H_7O + NO_2[a]	2.7×10^{-12}	−360				
i-$C_3H_7O_2$ + NO → i-$C_3H_7ONO_2$	fitted	parameters				
2 i-$C_3H_7O_2$ → 2 i-C_3H_7O + O_2[b]	1.3×10^{-12}	2240				
2 i-$C_3H_7O_2$ → $CH_3C(O)CH_3$ + i-C_3H_7OH[b]	9.7×10^{-13}	2240				
i-$C_3H_7O_2$ + NO_2 → i-$C_3H_7O_2NO_2$[c]	4.7×10^{-13}	−620				
i-$C_3H_7O_2$ + HO_2 → i-C_3H_7OOH + O_2[d]	7.5×10^{-13}	−700				
i-C_3H_7O → CH_3CHO + CH_3[e]	1.0×10^{15}	8807				
i-C_3H_7O + O_2 → $CH_3C(O)CH_3$ + HO_2[f]	1.4×10^{-14}	210				
i-C_3H_7O + NO → i-C_3H_7ONO[g]	8.9×10^{-12}	−397				
i-C_3H_7O + NO_2 → i-$C_3H_7ONO_2$[h]			2.0×10^{-27}	4	3.3×10^{-11}	1
CH_3 + O_2 → CH_3O_2[i]			4.50×10^{-31}	3	1.8×10^{-12}	1.7
CH_3O_2 + NO → CH_3O + NO_2[j]	9.2×10^{-13}	−600				
HO_2 + NO → OH + NO_2[i]	3.5×10^{-12}	−250				
HO_2 + OH → H_2O + O_2[i]	4.8×10^{-11}	−250				
OH + OH → H_2O_2[i]			6.2×10^{-31}	1	2.6×10^{-11}	0
OH + NO → HONO[i]			7.0×10^{-31}	2.6	3.6×10^{-11}	0.1
OH + NO_2 → HNO_3[i]			2.5×10^{-30}	4.4	1.6×10^{-11}	1.7
OH+ $CH_3C(O)CH_3$ → $CH_3C(O)CH_2$ + H_2O[k]	1.25×10^{-12}	561				
OH + i-C_3H_7OH → i-C_3H_6OH + H_2O[l]	2.7×10^{-12}	−190				
OH + C_3H_6 → C_3H_6OH[m]	4.86×10^{-12}	−504				
C_3H_6OH + O_2 → $CH_3CH(O_2)CH_2OH$[n]	1.2×10^{-11}	0				
$CH_3CH(O_2)CH_2OH$ + NO → $CH_3CH(O)CH_2OH$ + NO_2[o]	1.0×10^{-11}	0				

[a] Eberhard, J.; Villalta, P. W.; Howard, C. J. *J. Phys. Chem.* **1996**, *100*, 993. [b] Wallington, T. J.; Dagaut, P.; Kurylo, M. J. *Chem. Rev.* **1992**, *92*, 667. [c] From $C_2H_5O_2$ + NO_2 value, Ranschaert, D. L.; Schneider, N. J.; Elrod, M. J. *J. Phys. Chem. A.* **2000**, *104*, 5758. [d] From $C_2H_5O_2$ + HO_2 value, DeMore, W. B.; Sander, S. P.; Howard, C. J.; Ravishankara, A. R.; Golden, D. M.; Kolb, C. E.; Hampson, R. F.; Kurylo, M. J.; Molina, M. J. *Chemical Kinetics and Photochemical Data for Use in Stratospheric Modeling*, *JPL Publication 97-4*; Jet Propulsion Laboratory: Pasadena, CA, 1997. [e] First order rate constant, Heicklen, J. *Adv. Photochem.* **1988**, *14*, 177. [f] Atkinson, R.; Baulch, D. L.; Cox, R. A.; Hampson, R. F.; Kerr, J. A.; Rossi, M. J.; Troe, J. *Summary of Evaluated Kinetic Data for Atmospheric Chemistry* (http://www.iupac-kinetic.ch.cam.ac.uk); IUPAC Subcommittee on Gas Kinetic Data Evaluation for Atmospheric Chemistry: Cambridge, U.K., 2001. [g] Fittschen, C.; Frenzel, A.; Imrik, K.; Devolder, P. *Int. J. Chem. Kinet.* **1999**, *31*, 860. [h] k_∞^{300} from Mund, C.; Fockenberg, C.; Zellner, R. *Ber. Bunsenges. Phys. Chem.* **1998**, *102*, 709, temperature dependence from C_2H_5O + NO_2 , DeMore, W. B.; Sander, S. P.; Howard, C. J; Ravishankara, A. R.; Golden, D. M.; Kolb, C. E.; Hampson, R. F; Kurylo, M. J.; Molina, M. J. *Chemical Kinetics and Photochemical Data for Use in Stratospheric Modeling*, *JPL Publication 97-4*; Jet Propulsion Laboratory: Pasadena, CA, 1997. [i] DeMore, W. B.; Sander, S. P.; Howard, C. J; Ravishankara, A. R.; Golden, D. M.; Kolb, C. E.; Hampson, R. F; Kurylo, M. J.; Molina, M. J. *Chemical Kinetics and Photochemical Data for Use in Stratospheric Modeling*, *JPL Publication 97-4*; Jet Propulsion Laboratory: Pasadena, CA, 1997. [j] Scholtens, K. W.; Messer, B. M.; Cappa, C. D.; Elrod, M. J. *J. Phys. Chem. A* **1999**, *103*, 4378. [k] Le Calve, S.; Hitier, D.; Le Bras, G.; Mellouki, A. *J. Phys. Chem. A* **1998**, *102*, 4579. [l] Atkinson, R.; Baulch, D. L.; Cox, R. A.; Hampson, R. F.; Kerr, J. A.; Rossi, M. J.; Troe, J. *Summary of Evaluated Kinetic Data for Atmospheric Chemistry* (http://www.iupac-kinetic.ch.cam.ac.uk); IUPAC Subcommittee on Gas Kinetic Data Evaluation for Atmospheric Chemistry: Cambridge, U.K., 2001. [m] Tsang, W. *J. Phys. Chem. Ref. Data* **1991**, *20*, 221. [n] Miyoshi, A.; Matsui, H.; Washida, N. *J. Phys. Chem.* **1990**, *94*, 3016. [o] Average alkyl peroxy + NO rate constant, Wallington, T. J.; Dagaut, P.; Kurylo, M. J.; *Chem. Rev.* **1992**, *92*, 667. [p] Pressure independent rate constants calculated from $k(T) = Ae^{-E_a/RT}$. Pressure dependent rate constants calculated from $k([M],T) = \{k_0(T)[M]/[1 + (k_0(T)[M]/k_\infty(T))]\} \times 0.6^{\{1+[\log_{10}(k_0(T)[M]/k_\infty(T))]^2\}^{-1}}$ where $k_0(T) = k_0^{300}(T/300)^{-n}$ and $k_\infty(T) = k_\infty^{300}(T/300)^{-m}$.

studies.[7−11] Because of the excellent linearity of the pseudo-first-order decays and the agreement with previous rate constant determinations for this method, we conclude that plug flow approximation holds well for the $C_3H_7O_2$ + NO system under our flow conditions.

Temperature Dependence of the Overall Rate Constant (k_6) for $C_3H_7O_2$ + NO. We performed several measurements at 100 Torr pressure and at temperatures between 298 and 213 K in order to establish the temperature dependence of the rate constant for conditions relevant to the upper troposphere. The rate constant increased by approximately 40% as the temperature was lowered over this range. From the data listed in Table 1 and plotted in Figure 4, we obtained the Arrhenius expression $k(T) = 4.3^{+1.0}_{-0.9} \times 10^{-12}$ exp[(268 ± 56)/T] cm^3 $molecule^{-1}$ s^{-1}. Within the stated uncertainties of the experiments, our temperature dependence is in agreement with the results of Howard and co-workers for their measurement of the temperature dependence of the overall rate for n-$C_3H_7O_2$ + NO and i-$C_3H_7O_2$ + NO reactions, which were made about 1 Torr pressure.[8;9] Because of this good agreement with specific isomer $C_3H_7O_2$ + NO experiments of Howard and co-workers and because our main intent in measuring the temperature dependent overall rate constant was to provide an internally consistent method for calculating the nitrate branching ratios, we did not pursue the measurement of the isomer-specific overall rate constants.

***i*-$C_3H_7ONO_2$ Branching Ratio Determination.** We were able to observe the production of very small concentrations of i-$C_3H_7ONO_2$ (∼4.0×10^9 molecule cm^{-3}) over the reaction time (∼30 ms), which we have positively identified as coming from reaction 11b. In Figure 5, the i-$C_3H_7ONO_2$ rise (squares) has been overlaid on the background signal (circles) to demonstrate that the i-$C_3H_7ONO_2$ rise is significantly larger than the ±2σ level of the background signal. Under the experimental conditions shown in Figure 5, kinetics modeling shows that the i-C_3H_7O + NO_2 side reaction can produce concentrations of i-$C_3H_7ONO_2$ that are on the order of the detection level of the instrument (∼5.0×10^8 molecule cm^{-3}) and are less than the actual i-$C_3H_7ONO_2$ observed (∼4.3×10^9 molecule cm^{-3}). Table 2 contains a list of the reactions used in the modeling. An inspection of Table 2 indicates that only one side reaction directly produces i-$C_3H_7ONO_2$

$$i\text{-}C_3H_7O + NO_2 + M \rightarrow i\text{-}C_3H_7ONO_2 + M \qquad (12)$$

However, this reaction is significant in that the reactants are the products of the dominant reaction channel for i-$C_3H_7O_2$ + NO. As mentioned in the Experimental Section, oxygen was

TABLE 3: Branching Ratio Data for the *i*-$C_3H_7O_2$ + NO Reaction at 100 Torr Pressure

T (K)	velocity (cm s^{-1})	Reynold's no.	$[i\text{-}C_3H_7O_2]_0$ (10^{11} molecule cm^{-3})	$[NO]_0$ (10^{11} molecule cm^{-3})	k_{11b} (10^{-14} cm^3 molecule^{-1} s^{-1})	branching ratio $k_{11b}/(k_{11a}+k_{11b})$
298	1280	2450	6.9	36	5.4	0.006
298	1280	2450	6.9	55	2.7	0.003
298	1280	2450	6.9	46	6.8	0.008
298	1280	2450	6.9	36	4.5	0.005
298	1280	2450	6.9	36	6.8	0.008
298	1300	2470	3.3	35	6.3	0.007
298	1300	2470	3.3	46	3.6	0.004
298	1300	2470	3.3	55	3.6	0.004
298	1300	2470	3.3	55	4.5	0.005
298	1300	2470	3.3	33	4.5	0.005
298	1300	2470	3.3	46	3.6	0.004
298	1300	2470	3.3	46	3.6	0.004
298	1300	2470	3.3	52	5.4	0.006
298	1300	2470	3.3	52	7.2	0.008
263	1160	2710	3.3	38	13	0.012
253	1120	2800	2.7	51	7.8	0.007
253	1120	2800	2.7	41	13	0.012
243	1100	2900	3.4	46	24	0.020
243	1100	2860	3.4	46	23	0.019
233	1180	3310	4.1	50	25	0.020
233	1110	3250	5.0	31	17	0.013
233	1110	3250	5.0	17	11	0.009
233	1270	3670	5.0	28	14	0.011
233	1270	3670	5.0	21	14	0.011
223	1180	3660	3.4	46	41	0.030
223	1180	3630	3.4	46	35	0.026
223	1290	3840	5.3	35	34	0.025
223	1290	3840	5.3	28	18	0.013
223	1290	3840	5.3	22	22	0.016
213	1280	4120	5.0	33	18	0.012
213	1280	4120	5.0	33	21	0.014
213	1440	4580	5.0	29	29	0.020
213	1440	4580	5.0	20	31	0.021

added at higher concentrations in the branching ratio experiments so that the following reaction was favored

$$i\text{-}C_3H_7O + O_2 \rightarrow CH_3C(O)CH_3 + HO_2 \qquad (13)$$

which effectively scavenges *i*-C_3H_7O from the system. As described in the Experimental Section, two sets of experiments were done at O_2 concentrations of 5.0×10^{17} and 1.0×10^{18} molecule cm^{-3} to examine potential interferences from this reaction. Both sets yielded the same results, indicating that the production of *i*-$C_3H_7ONO_2$ from reaction 12 was minimized under the high O_2 concentrations used in the branching ratio experiments.

Computer modeling was used to extract a rate constant for reaction 11b by fitting the observed *i*-$C_3H_7ONO_2$ production. The actual time profile of the *i*-$C_3H_7ONO_2$ production, as well as the total production of i-$C_3H_7ONO_2$ over the total reaction time were used as constraints in the fitting process. The model input included the concentrations of $C_3H_7O_2$, NO, and all precursors. Table 3 contains a list of the initial conditions and calculated rate constants (k_{11b}) for the branching ratio experiments. As stated earlier, we believe that the relevant experimental uncertainty for a rate constant determination with this apparatus is on the order of 30%, although the uncertainty may be somewhat higher because the branching ratio measurements are being made very close to the detection level of the instrument. In addition, the branching ratio method requires the added step of titration and calibration experiments needed to determine $[C_3H_7O_2]_0$. The uncertainty in the rate constant for reaction 12 is expected to play the largest role in the propagation of rate constant uncertainties through our fitting process. The room-temperature uncertainty in k_{12} is only 10%,[21] but the temperature dependence of k_{12} has not been directly measured (the temperature dependence of the $C_2H_5O + NO_2$ reaction is used as an estimate in the modeling calculations). Propagating the 10% value through our model indicates that this uncertainty has a minor effect (less than 5%) on our fitted value for k_{11b}. However, because the lower temperature measurements might be subject to higher uncertainty, we estimate the total error to be approximately 50% for the branching ratio measurements.

We performed several measurements of the *i*-$C_3H_7ONO_2$-producing branching ratio at temperatures between 213 and 298 K in order to establish the temperature dependence of the rate constant k_{11b} for conditions relevant to the upper troposphere. From the data listed in Table 3 and presented in Figure 6, the following Arrhenius expression is obtained for the experiments performed at 100 Torr total pressure: $4.9^{+5.3}_{-2.9} \times 10^{-16}$ $\exp[(1380 \pm 230)/T]$ cm^3 molecule^{-1} s^{-1}. Again, the uncertainty represents the two standard deviation statistical error in the data and is not an estimate of systematic errors (which are discussed above). The branching ratios $[k_{11b}/(k_{11a}+k_{11b})]$ reported in Table 3 were calculated using the Arrhenius parameters for the overall rate constant ($k_{11a}+k_{11b}$) for *i*-$C_3H_7O_2$ + NO given in Table 2. The branching ratios range from about 0.006 at 298 K to 0.02 at 213 K, indicating the increased importance of the *i*-$C_3H_7ONO_2$-producing channel at lower temperatures. Because the *i*-$C_3H_7ONO_2$-producing channel is almost certainly pressure-dependent, it would be of interest to attempt to establish the pressure dependence of the rate constant. However, because the measurements made at 100 Torr were barely within the detection limit of the instrument, it was not surprising that we were unable to obtain sufficient sensitivity to pursue experiments at pressures other than 100 Torr. It would also be of interest to pursue the kinetics of the *n*-$C_3H_7ONO_2$-producing reaction. However, we

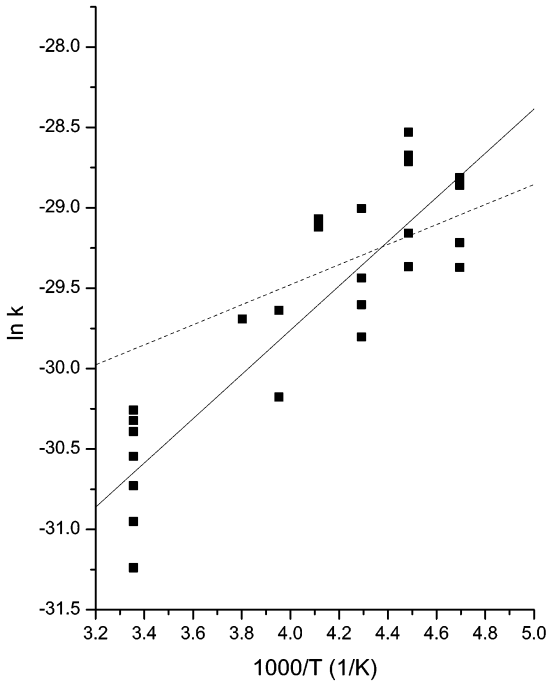

Figure 6. Arrhenius plots of the temperature dependence of the rate constant of the *i*-$C_3H_7ONO_2$ branching channel for the present work (data points and solid line) and from the predictions of the Atkinson model (dotted line) at 100 Torr pressure.

are not aware of a discharge flow method to allow for the selective generation of *n*-$C_3H_7O_2$.

In Figure 6, the temperature-dependent *i*-$C_3H_7ONO_2$-producing rate constant (k_{11b}) obtained in the present work is compared to the predictions from the Atkinson model[2] at a total pressure of 100 Torr. The model predicts a 298 K, 100 Torr branching ratio of about 0.009, which is within the estimated uncertainty of our experimental value of 0.006. The pressure dependence of the *i*-$C_3H_7ONO_2$ branching channel observed from the present 100 Torr results and the 735 Torr results of Atkinson and coworkers is consistent with this reaction being in the third-order limit in this pressure range. All in all, the performance of empirical model is an impressive extrapolation, given that the pressure and temperature dependence has been derived from experimental results for the larger C_5-C_7 systems. However, it is again worth noting that our previous results for the $C_2H_5ONO_2$ branching ratios were in somewhat poorer agreement with the Atkinson model results.[5]

In our previous work on the $C_2H_5ONO_2$ branching ratio for the $C_2H_5O_2$ + NO reaction, we used our branching ratio results and the Bertman et al. model[13] described in the Introduction to provide further support for the conclusion that field measurements of $C_2H_5ONO_2$ were not consistent with ethane oxidation chemistry as the sole source of this species.[5] In fact, the calculation indicated that ethane was probably responsible for less than 10% of the $C_2H_5ONO_2$ present in the atmosphere. The measurements presented here serve to provide further confidence in the Atkinson model used by Bertman et al. for the calculation of *i*-$C_3H_7ONO_2$ from the *i*-$C_3H_7O_2$ + NO reaction and, thus, support the conclusion that some atmospheric *i*-$C_3H_7ONO_2$ is produced via the oxidation of larger hydrocarbons.[13;24]

Conclusions

The results presented here represent the first temperature dependence measurements of the *i*-$C_3H_7ONO_2$-producing rate constant from the *i*-$C_3H_7O_2$ + NO reaction, as well as measurements of the temperature dependence of the overall rate constant for the reaction of $C_3H_7O_2$ with NO. Our measurement of the temperature dependence of the overall rate constant at 100 Torr for the $C_3H_7O_2$ + NO reaction was found to be in good agreement with previous measurements performed at lower pressures.[8,9] The branching ratio [$k_{11b}/(k_{11a} + k_{11b})$] at 100 Torr pressure for *i*-$C_3H_7ONO_2$ formation was determined to be about 0.006 at 298 K and was found to increase to about 0.02 at 213 K. The temperature-dependent rate constant k_{11b} was accurately predicted by extrapolating from a model based on organic nitrate formation from C_3-C_8 hydrocarbon systems.[2] The present work is useful for (a) obtaining the *i*-$C_3H_7ONO_2$ yield data for conditions representative of the upper troposphere (210 K and 100 torr pressure) and (b) when the present 298 K and 100 torr pressure yield is combined with previous atmospheric pressure data at 299 K, constraints concerning the pressure dependence are placed on theoretical models of alkyl nitrate formation from the RO_2 + NO reactions.

Acknowledgment. The authors acknowledge experimental assistance from Nick Schneider and Andy Huisman. This material is based upon work supported by the National Science Foundation under Grant No. 0196205.

References and Notes

(1) Brasseur, G. P.; Orlando, J. J.; Tyndall, G. S. *Atmospheric Chemistry and Global Change*; Oxford University Press: New York, 1999.
(2) Arey, J.; Aschmann, S. M.; Kwok, E. S. C.; Atkinson, R. *J. Phys. Chem* **2001**, *105*, 1020−1027.
(3) Carter, W. P. L.; Atkinson, R. *J. Atmos. Chem.* **1989**, *8*, 165.
(4) Scholtens, K. W.; Messer, B. M.; Cappa, C. D.; Elrod, M. J. *J. Phys. Chem. A* **1999**, *103*, 4378.
(5) Ranschaert, D. L.; Schneider, N. J.; Elrod, M. J. *J. Phys. Chem. A* **2000**, *104*, 5758.
(6) Droge, A. T.; Tully, F. P. *J. Phys. Chem.* **1986**, *90*, 1949.
(7) Eberhard, J.; Howard, C. J. *J. Phys. Chem.* **1997**, *101*, 3360−3366.
(8) Eberhard, J.; Howard, C. J. *Int. J. Chem. Kinet.* **1996**, *28*, 731−740.
(9) Eberhard, J.; Villalta, P. W.; Howard, C. J. *J. Phys. Chem.* **1996**, *100*, 993−997.
(10) Peeters, J.; Vertommen, J.; Langhans, I. *Ber. Bunsen-Ges. Phys. Chem.* **1992**, *96*, 431−436.
(11) Adachi, H.; Basco, N. *Int. J. Chem. Kinet.* **1982**, *14*, 1243−1251.
(12) Atkinson, R.; Aschmann, S. M.; Carter, W. P. L.; Winer, A. M.; Pitts, J. N., Jr. *J. Phys. Chem.* **1982**, *86*, 4563−4569.
(13) Bertman, S. B.; Roberts, J. M.; Parrish, D. D.; Buhr, M. P.; Goldan, P. D.; Kuster, W. C.; Fehsenfeld, F. C.; Montzka, S. A.; Westberg, H. *J. Geophys. Res.* **1995**, *100*, 22805.
(14) Seeley, J. V.; Jayne, J. T.; Molina, M. J. *Int. J. Chem. Kinet.* **1993**, *25*, 571.
(15) Seeley, J. V. *Experimental Studies of Gas-Phase Radical Reactions Using the Turbulent Flow Tube Technique*; Massachusetts Institute of Technology: Cambridge, MA, 1994.
(16) DeMore, W. B.; Sander, S. P.; Howard, C. J.; Ravishankara, A. R.; Golden, D. M.; Kolb, C. E.; Hampson, R. F.; Kurylo, M. J.; Molina, M. J. *Chemical Kinetics and Photochemical Data for Use in Stratospheric Modeling, JPL Publication 97-4*; Jet Propulsion Laboratory: Pasadena, CA, 1997.
(17) Atkinson, R.; Baulch, D. L.; Cox, R. A.; Hampson, R. F.; Kerr, J. A.; Rossi, M. J.; Troe, J. *IUPAC Subcommittee on Gas Kinetic Data Evaluation for Atmospheric Chemistry*; 1999.
(18) Tschuikow-Roux, E.; Yano, T.; Niedzielski, J. *J. Chem. Phys.* **1985**, *82*, 65.
(19) Harris, G. W.; Pitts, J. N. *J. Chem. Phys.* **1982**, *77*, 3994.
(20) Fittschen, C.; Frenzel, A.; Imrik, K.; Devolder, P. *Int. J. Chem. Kinet.* **1999**, *31*, 860.
(21) Mund, C.; Fockenberg, C.; Zellner, R. *Ber. Bunsen-Ges. Phys. Chem.* **1998**, *102*, 709.
(22) Messer, B. M.; Stielstra, D. E.; Cappa, C. D.; Scholtens, K. W.; Elrod, M. J. *Int. J. Mass Spectrom.* **2000**, *197*, 219.
(23) Huey, L. G.; Hanson, D. R.; Howard, C. J. *J. Phys. Chem.* **1995**, *99*, 5001.
(24) Flocke, F.; Volz-Thomas, A.; Buers, H. J.; Patz, W.; Garthe, H. J.; Kley, D. *J. Geophys. Res. Atmospheres* **1998**, *103*, 5729.